



## OPEN ACCESS

## EDITED BY

Yudong Liu,  
Institute of Geriatric Medicine, Chinese  
Academy of Medical Sciences, China

## REVIEWED BY

Julia Weinmann-Menke,  
Johannes Gutenberg University  
Mainz, Germany  
Roi Avraham,  
Weizmann Institute of Science, Israel

## \*CORRESPONDENCE

Pawel Paszek  
pawel.paszek@manchester.ac.uk

†These authors have contributed  
equally to this work

## SPECIALTY SECTION

This article was submitted to  
Systems Immunology,  
a section of the journal  
Frontiers in Immunology

RECEIVED 18 May 2022

ACCEPTED 08 September 2022

PUBLISHED 27 September 2022

## CITATION

Kalliara E, Kardynska M, Bagnall J,  
Spiller DG, Müller W, Ruckerl D,  
Śmieja J, Biswas SK and Paszek P  
(2022) Post-transcriptional regulatory  
feedback encodes JAK-STAT signal  
memory of interferon stimulation.  
*Front. Immunol.* 13:947213.  
doi: 10.3389/fimmu.2022.947213

## COPYRIGHT

© 2022 Kalliara, Kardynska, Bagnall,  
Spiller, Müller, Ruckerl, Śmieja, Biswas  
and Paszek. This is an open-access  
article distributed under the terms of  
the [Creative Commons Attribution  
License \(CC BY\)](https://creativecommons.org/licenses/by/4.0/). The use, distribution  
or reproduction in other forums is  
permitted, provided the original  
author(s) and the copyright owner(s)  
are credited and that the original  
publication in this journal is cited, in  
accordance with accepted academic  
practice. No use, distribution or  
reproduction is permitted which  
does not comply with these terms.

# Post-transcriptional regulatory feedback encodes JAK-STAT signal memory of interferon stimulation

Eirini Kalliara<sup>1,2†</sup>, Malgorzata Kardynska<sup>3,4†</sup>, James Bagnall<sup>1</sup>,  
David G. Spiller<sup>1</sup>, Werner Müller<sup>1</sup>, Dominik Ruckerl<sup>1</sup>,  
Jarosław Śmieja<sup>4</sup>, Subhra K. Biswas<sup>2</sup> and Pawel Paszek<sup>1\*</sup>

<sup>1</sup>School of Biology, Faculty of Biology, Medicine and Health, University of Manchester, Manchester Academic Health Science Centre, Manchester, United Kingdom, <sup>2</sup>Singapore Immunology Network, Agency for Science, Technology and Research (A\*STAR), Singapore, Singapore, <sup>3</sup>Department of Biosensors and Processing of Biomedical Signals, Silesian University of Technology, Zabrze, Poland, <sup>4</sup>Department of Systems Biology and Engineering, Silesian University of Technology, Gliwice, Poland

Immune cells fine tune their responses to infection and inflammatory cues. Here, using live-cell confocal microscopy and mathematical modelling, we investigate interferon-induced JAK-STAT signalling in innate immune macrophages. We demonstrate that transient exposure to IFN- $\gamma$  stimulation induces a long-term desensitisation of STAT1 signalling and gene expression responses, revealing a dose- and time-dependent regulatory feedback that controls JAK-STAT responses upon re-exposure to stimulus. We show that IFN- $\alpha/\beta$ 1 elicit different level of desensitisation from IFN- $\gamma$ , where cells refractory to IFN- $\alpha/\beta$ 1 are sensitive to IFN- $\gamma$ , but not *vice versa*. We experimentally demonstrate that the underlying feedback mechanism involves regulation of STAT1 phosphorylation but is independent of new mRNA synthesis and cognate receptor expression. A new feedback model of the protein tyrosine phosphatase activity recapitulates experimental data and demonstrates JAK-STAT network's ability to decode relative changes of dose, timing, and type of temporal interferon stimulation. These findings reveal that STAT desensitisation renders cells with signalling memory of type I and II interferon stimulation, which in the future may improve administration of interferon therapy.

## KEYWORDS

JAK-STAT network, STAT1 kinetics, interferons, pathway desensitisation, mathematical modelling, signal memory, live-cell microscopy

## Introduction

Immune signaling systems decode external signals in order to produce appropriate responses (1). Underlying mechanisms involve complex regulatory networks with feedback loops that generate outputs depending on the signal type, strength, or duration (2, 3). For example, the temporal responses of the nuclear factor- $\kappa$ B (NF- $\kappa$ B) transcription factor encode different pathogen-derived molecules and cytokines of the immune system (4–6) and adapts to rapidly changing inflammatory cues (7–11). The emergent properties of the cellular signaling networks serve as a paradigm to understand how immune cells process inflammatory cues (12).

Interferons (IFNs) are secreted signaling molecules with antiviral, antiproliferative and immunomodulatory functions in response to infection (13). IFN- $\gamma$  is a type II interferon, produced by innate immune natural killer cells and innate lymphoid cells as well as T lymphocytes of the adaptive immunity, mainly, but not only, in the direct response to pathogens (14). Innate immune macrophages are the main physiological target of newly secreted IFN- $\gamma$  (15). IFN- $\gamma$  exerts its biological function through binding to its cognate receptor (IFN- $\gamma$ R), which activates Janus kinase (JAK)-STAT signaling pathway (16). IFN- $\gamma$  binding leads to the nuclear translocation of Signal Transducers and Regulators of Transcription 1 (STAT) homodimers, which directly activate expression of hundreds of interferon-regulated genes (ISGs) *via* conserved sequences in their promoters (17). Functionally related type I interferons, such as IFN- $\alpha$  and IFN- $\beta$  regulate overlapping sets of genes *via* ISGs (in part through STAT1 homodimers), but also utilize IFN-stimulated response elements (through STAT1-STAT2-IRF9 complexes) (18). Regulation of IFN signaling exemplifies the intricate balance within the immune system to produce appropriate responses. A lack of IFN- $\gamma$  responses results in susceptibility to pathogen infection (19, 20), thus IFN- $\gamma$  has been clinically used to treat inflammation including sepsis (21). In turn, a sustained IFN signature has been associated with autoinflammatory diseases such as arthritis (14) or cancer (17) and uncontrolled type I IFN responses have also recently been associated with severe COVID 19 symptoms (22, 23). The properties of the JAK-STAT network are controlled *via* the temporal regulation of STAT activity *via* the receptor availability (24) and regulatory feedback (16). Known feedback mechanisms involve transcriptional activation of Suppressors of Cytokine Signalling (SOCS), protein inhibitor of activated STAT (PIAS) and ubiquitin-specific peptidase (USP18) (14, 25–29) as well as post-translational regulation of tyrosine phosphatase activity (30). To achieve the appropriate level of response, innate immune cells acquired the ability to adapt to repeated immune challenges, i.e., ‘memory’ (31). IFN- $\gamma$  sensitizes cells for subsequent stimulation through long-term epigenetic changes (32) as well as regulation of STAT expression (33). In contrast, pathway desensitization represents a mechanism that prevents prolonged or uncontrolled activation to persistent

stimulation. Best characterized examples involve endotoxin resistance in the toll-like receptor system (34, 35), however desensitization has also been extensively studied for type I interferon signaling (25, 26, 36). How cells adapt to temporal IFN- $\gamma$  stimulation is less understood.

In this work, we use live-cell confocal microscopy and mathematical modelling to investigate STAT1 responses to IFNs in innate immune macrophages. Using pulses of IFN- $\gamma$  and IFN- $\alpha/\beta$ 1 at different concentrations and frequency we demonstrate a long-term dose-, time- and stimulus- specific desensitization of STAT1 signaling and gene expression responses. We demonstrate that pathway desensitization involves control of STAT1 phosphorylation and is independent of new mRNA synthesis and IFN $\gamma$ R expression. Our new dynamical mathematical model of the JAK-STAT signaling network that recapitulates our experimental data, demonstrates that stimuli-induced STAT1 desensitization renders cells with signaling memory of IFN stimulation. These analyses reveal the ability of macrophages to quantitatively fine-tune their responses to temporal interferon stimulation.

## Materials and methods

### Cells and reagents

Immortalized bone marrow-derived mouse macrophage (iBMDM) cells (37) were cultured in Dulbecco’s Modified Eagle Medium (DMEM) with L-glutamine (Sigma-Aldrich), supplemented with 10% (v/v) of heat-inactivated Foetal Bovine Serum (Life Technologies Ltd) and 1% (v/v) of Penicillin-Streptomycin (Sigma-Aldrich) solution. Cells were cultured between passages 6–30 in sterile Nunc™ 10 cm cell culture petri dishes (ThermoFisher Scientific) till 80–90% confluent. Lentiviral transduction (38) was used to develop reporter iBMDM line expressing murine STAT1 coding sequence C-terminally fused with the red fluorescent protein (STAT1-tagRFP) and murine STAT6 coding sequence N-terminally fused with yellow fluorescent protein (Venus-STAT6). Additionally, cells expressed histone H2B protein fused with cyan fluorescent protein (AmCyan-H2B). iBMDMs were sequentially transduced and triple positive cells were identified using fluorescence single cell sorter (BD Influx) to derive a clonal reporter line. Cells were stimulated with recombinant mouse IFN- $\gamma$  (575306, Biolegend), IL-4 (574306, Biolegend), IFN- $\alpha$  (752802, Biolegend) and IFN- $\beta$ 1 (581302, Biolegend).

### Confocal microscopy and image analysis

Fluorescent confocal imaging was performed with Zeiss LSM 710, LSM 780 and LSM 880 laser scanning confocal microscopes,

which collect emitted signals using dichroic mirrors and band-pass filters or spectral separation and detector arrays. Fluorophores were excited with the appropriate laser lines (AmCyan excited with 458 nm laser line, Venus with 514 nm laser line, tagRFP with 561 nm laser line). Imaging was conducted using Fluar 40x NA 1.3 (oil immersion) objective using Zen 2010b SP1 software. Time-lapse images were performed by seeding cells onto 1-compartment or 4-compartment round glass-bottom 35 mm culture dishes (627860 & 627870, Greiner Bio-One) at density of  $300 \times 10^3$  cells/dish or  $100 \times 10^3$  cells/compartment, respectively. Imaging plates were placed on the microscope stage in a humidified incubator maintaining 37 °C and 5% CO<sub>2</sub>. Image series were captured with a time interval of 5 mins by selecting several regions of interest per condition. Image analysis was performed using Imaris Bitlane software version 9.3 using AmCyan fluorescent signal as a nuclear mask to segment and track single cells. Nuclear masking was tailored according to nuclei size and cell movement depending on the experimental conditions. Automated cell tracking was executed by Autoregressive Motion Imaris algorithm. Quantified data were extracted as mean fluorescence intensity for the respective fluorescent channels under investigation. The values were imported to GraphPad Prism 9 for further processing and statistical analyses.

## Live-cell luminometry

Lentiviral GAS-luciferase reporter (GAS-luc) construct was generated from the previously described 5κB-Luc plasmid (39). Namely, PacI and XhoI restriction sites were used to replace κB elements with a GAS consensus sequence (AGTTTCATATTA CTCTAAATCAGTTTCATATTACTCTAAATCAGTTTCATA T T A C T C T A A A T C A G T T T C A T A T T A C T C T A A A T C A G T T T C A T A T T A C T C T A A A T C A G T T T C A T A T T A C T C T A A A T C) (40). Lentivirus production and transduction of iBMDMs were carried out as previously described (38). For the purposes of live-cell luminometry  $10 \times 10^3$  GAS-luc cells were seeded onto white, flat-bottom 12-well culture microplates (Greiner Bio-one) in 1 ml complete medium. 10 μl of 100 mM D-luciferin (Biosynth) was added 24 h prior to the start of the assay. Live-cell luminometry was performed using a Fluostar Omega luminometer (BMG Labtech) at 37 °C and 5% CO<sub>2</sub>. Light production was measured at 492 nm with 10 mins intervals for 24 h.

## Single molecule RNA-FISH

Custom smFISH probes were designed using Stellaris Probe Designer version 4.2 (Biosearch Technologies Inc.) against murine STAT1 (NM\_001205313) and SOCS1 (NM\_001271603) (see

Table S1 for the probe sets). Each probe was attached with a fluorophore (either Quasar 570 or Quasar 670). Cells were seeded onto 18 mm coverslips (BDH) placed in 6-well or 12-well plates (Corning, Appleton Woods Limited). For the measurement, cells were washed with PBS and fixed with 4% formaldehyde (Sigma-Aldrich) for 10 mins. Subsequently, cells were permeabilized with 70% Ethanol (EtOH) and left for at least 1 h at 4°C according to Stellaris protocol for adherent cells (41). Probe hybridization was performed at a concentration of 125 nM for up to 16 h at 37 °C in a humidified chamber. Coverslips were mounted on microscope slides (ThermoFisher) using Vectashield mounting medium (Vector Laboratories) containing 4', 6-diaminidino-2-phenylindole (DAPI) for nuclei staining. Imaging was performed using Deltavision deconvolution system equipped with a Plan Apo 60x 1.42 NA (oil immersion) objective. Light-emitting diodes were used to illuminate specimens with the desired excitation wavelength band (358 nm for DAPI, 570 nm for Quasar 570 and 670 nm for Quasar 670). Images were acquired as z-series with an optical spacing of 0.2 μm using MetaMorph acquisition software, respectively. Obtained images were deconvolved using Huygens Professional software. mRNA quantification was performed in FISHQuant (42).

## qRT-PCR

Cells were seeded onto 6-well plates with a density of  $300 \times 10^3$  cells/well. RNA extraction was performed using Qiagen RNeasy mini kit according to manufacturer instructions. RNA concentration was quantified using a NanoDrop 1000 Spectrophotometer (Thermo Fisher Scientific). 1 μg of RNA was used for reverse transcription using the SensiFAST cDNA synthesis kit (Bioline). qPCR reactions were prepared in MicroAmp Fast Optical 96-well plates with barcode (Applied Biosystems) using SYBR Green master mix (Applied Biosystems). A 10 μl final volume reaction was prepared, which included 5 μl of the SYBR Green master mix, 0.5 μl of primer, 0.5 μl of the cDNA template and 3.5 μl of sterile DNase-free water. Amplification was performed using the StepOne Plus Real-Time thermal cycler (Applied Biosystems). Amplification of β-actin gene was used as a control across all samples. Genes of interest were first normalized to β-actin expression within the same sample. Normalized expression of target genes in the samples of interest were then compared to the normalized expression of the same genes in a reference control sample (untreated cells). Final levels of gene expression are presented as a fold change in the target sample compared to the reference/control sample ( $\Delta\Delta Ct$ ) following established methodology (43). All samples were examined in three technical replicates. The following primer sequences were used (5' to 3'): β-Actin TATCC ACCTTCCAGCAGATGT (forward) and AGCTCAGT AACAGTCCGCCTA (reverse); STAT1 TCATCCCGCA GAGAGAAC (forward) and TGAAACGACCTAGAAGTGAG

(reverse); PD-L1 GAAAGTCAATGCCCCATACC (forward) and ATTGAGAAGCATCCCCTCTG (reverse), SOCS1 GAGACCTCATCCCACCTCTC (forward) and AGACACAAGCTGCTACAACC (reverse), CXCL10 CACGTGTTGAGATCATTGCC (forward) and TCACTCCAGTTAAGGAGCCC (reverse), ARG1 CTGTCTTTTAGGGTTACGGC (forward) and CTCGAGGCTGTCTTTTGGAG (reverse) and TNFA, TGAGGTCAATCTGCCCAAGT (forward) and TGGACCCTGAGCCATAATCC (reverse).

## Immunoblotting

Cells were lysed in 80  $\mu$ l of radioimmunoprecipitation assay buffer (RIPA) (89900, ThermoFisher, Scientific) supplemented with Pierce Protease Inhibitor Mini tablets (A32953, ThermoFisher Scientific) as per manufacturer's instructions. Cell extracts were incubated for 15 mins on ice followed by centrifugation at 12000 rpm for 12-15 mins at 4 °C. Protein concentration of each sample was measured with Pierce Bicinchoninic acid (BCA) protein assay kit (23227, ThermoFisher Scientific) according to manufacturer's protocol. Polyacrylamide gel of 10% size pore was prepared using a 30% w/v Acrylamide stock solution (A2-0084, Geneflow). A 2x protein loading buffer was freshly prepared using 950  $\mu$ l of 2x Laemmli buffer (161-0737, Bio-Rad) mixed with 50  $\mu$ l of  $\beta$ -ME. 20  $\mu$ g of protein sample was mixed with the appropriate amount of protein loading buffer and sterile double distilled water (ddH<sub>2</sub>O). Diluted protein samples were denatured at 95°C for 5 mins and loaded onto the wells of polyacrylamide gel. 5  $\mu$ l of Precision Plus Protein Dual Colour (1610374, Bio-Rad) ladder was also loaded onto the gel and run alongside the samples to determine the molecular weight. Electrophoresis was performed at 120 V for 60-90 mins. Transfer of proteins was confirmed by staining of membranes with Ponceau S stain (0.1% w/v Ponceau S solution in 1% v/v Acetic acid). Membranes were washed in PBS-Tween 20 (PBS-T) for 5 mins three times and blocked in 5% non-fat powdered milk (Sigma-Aldrich) in PBS for 1 h at room temperature. Probing with primary antibodies was conducted o/v at 4 °C. The next day, membranes were washed in PBS-T for 5 mins three times to remove unbound primary antibody and subsequently blocked in HRP- conjugated secondary IgG antibody for 1 h at room temperature. Following incubation, excess of secondary antibody was removed by washing membranes in PBS-T for 5 mins three times. Pierce ECL Western Blotting Substrate (32106, ThermoFisher Scientific) was used to incubate membranes as per manufacturer's instructions. Luminescent signal was captured on Carestream Biomax Xar films (F5513, Sigma-Aldrich) using an automatic X-ray processor model JP-33 (JPI). Primary antibodies were purchased from Cell Signaling Technology®: STAT1 rabbit polyclonal antibody (9172S) used at 1:1000 dilution; phospho-STAT1 (pTyr701) (58D6 clone) rabbit monoclonal antibody

(9167S) at 1:1000 dilution; and  $\beta$ -actin (13E5 clone) rabbit monoclonal antibody (4970S) at 1:2000 dilution. Primary antibodies were detected with Horseradish Peroxidase (HRP)-conjugated goat anti-rabbit IgG (H+L) secondary antibody (65-6120, ThermoFisher Scientific) using 1:3000 dilution. Quantification of immunoblotting was performed in ImageJ software using the 'Measure' function with setting 'Mean gray value' applied to individual bands (relative to the  $\beta$ -actin loading control and including background control).

## FACS analysis of receptor expression

Cells were either untreated (control) or treated with continuous 100 ng/ml IFN- $\gamma$ , or 1 h pulse of 100 ng/ml of IFN- $\gamma$  or combined pulse of IFN- $\alpha/\beta$ 1 (50 ng/ml of each). After scraping, collected cell suspensions were centrifuged at 400 x g for 5 mins and resuspended in 5 ml of PBS. For each condition, 1 x 10<sup>6</sup> cells were transferred in FACs tubes (STEMCELL Technologies). First, cells were stained with viability dye (Zombie Aqua™ fixable viability dye, Biolegend) in 1:1000 dilution in PBS and they were incubated at room temperature, in the dark, for 15 mins. Cells were then washed with MACs buffer (0.5% BSA and 250  $\mu$ M EDTA in PBS) and centrifuged at 400 x g for 5 mins. Next, cells were stained with PE-conjugated primary antibodies against IFN $\gamma$ -R  $\alpha$  chain (clone GIR-208, Biolegend) and IFN $\gamma$ -R  $\beta$  chain (clone 2HUB-159, Biolegend) at a final concentration of 5  $\mu$ g/ml in MACs buffer. Incubation was performed at room temperature, in the dark, for 25-30 mins. Stained cells were then washed with MACs buffer and centrifuged at 400 x g for 5 mins. Unstained cells served as control. Subsequently, cells were fixed using 4% of paraformaldehyde (PFA) solution for 10 mins and washed with PBS and centrifuged at 400 x g for 5 mins. Finally, cells were resuspended in 500  $\mu$ l of PBS and kept at 4°C o/n. Samples were analyzed the next day using a BD Fortessa X20 flow cytometer. PE-conjugated IFN $\gamma$ -R  $\alpha$  and  $\beta$  antibodies were excited using a blue (488 nm) laser line, while viability dye was excited with a violet (405 nm) laser line. Data were analyzed using FlowJo (version 10.3.0) and statistical analysis was performed using GraphPad Prism 8 (version 8.4.2). Data are presented as Geometric mean of fluorescence intensity acquired from three repeated experiments.

## JAK-STAT model development

The JAK-STAT mathematical model incorporating type I and type II interferon signaling was developed based on the existing model of IFN- $\beta$  induced signaling pathway (29). The original model consisted of 37 ordinary differential equations (ODES), but some molecules which were not relevant for the current work were removed, these included action of

hypothetical protein Phy as well as TAP1 and LMP2 mRNA output. The model was subsequently expanded to incorporate additional variables and interactions, including extracellular IFN- $\alpha/\beta$ 1 and IFN- $\gamma$ , their cognate receptors as well as the activation and the action of PTP proteins, including formation of PTP complexes with STATs. Three auxiliary variables were created to model PTP activation, resulting in total of 37 ODEs. Model parameters were then fitted to recapitulate experimental data including all the time-lapse microscopy for IFN- $\gamma$  and IFN- $\alpha/\beta$ 1 stimulation as well as levels of STAT1 mRNA and protein (see [Tables S2 to S5](#) for model equations, parameters and initial conditions). Simulations were performed using MATLAB R2020b. To directly compare the experimental results with model simulations, nuclear STAT1-tagRFP trajectories were scaled from arbitrary fluorescence levels to number of molecules. First, baseline fluorescent levels were removed (by subtracting the minimum value in the dataset). Resulting levels were subsequently multiplied by a scaling factor to match the maximal level of nuclear STAT1 in simulations, across different experimental protocols.

## Statistical analyses

Statistical analysis was performed using GraphPad Prism 8 software (version 8.4.2). The D'Agostino-Pearson test was applied to test for normal (Gaussian) distribution of acquired data. Two-sample comparison was conducted using non-parametric Mann Whitney test, for analyses of variance Kruskal-Wallis ANOVA with Dunn's multiple comparisons test was performed. Non-parametric Spearman correlation was conducted to test association between two selected variables coefficient of correlation  $r$ .

## Results

### IFN- $\gamma$ induces desensitization of STAT1 signaling and gene expression responses

To investigate STAT signaling, we engineered a reporter murine immortalized bone marrow-derived macrophage (iBMDM) line (37) constitutively expressing STAT1 fused to red fluorescent protein (STAT1-tagRFP). Reporter cells also expressed the nuclear marker AmCyan-H2B to enable automated segmentation and tracking of confocal microscopy images. In addition, as a tool to study macrophage activation, reporter cells expressed STAT6 tagged with yellow fluorescent protein (Venus-STAT6). We focused on interferon signaling and assayed STAT1 activation *via* confocal microscopy. Untreated cells exhibited a predominant cytoplasmic localization of STAT1-tagRFP, but a continuous stimulation with a saturated dose of 100 ng/ml of IFN- $\gamma$  (see [Figure S1A](#) for a dose response)

resulted in a single transient nuclear STAT1 translocation ([Figures 1A, B](#) and [Video 1](#)). Cells exhibited a maximal STAT1-tag RFP nuclear localization at  $72 \pm 42$  mins (mean  $\pm$  standard deviation, SD) after the start of the experiment ([Figure 1C](#)). The translocation lasted for up to 6 h, after which nuclear STAT1-tagRFP levels returned towards the pre-stimulation steady-state. A transient activation in response to continuous treatment is a hallmark of desensitization, where cells become unresponsive to prolonged presence of stimulus (34, 35). In contrast, other signaling systems remain active if the stimulus is present, as in the case of the cytokine stimulation of the NF- $\kappa$ B system (9, 44, 45). To understand whether STAT1 signaling exhibited desensitization, we treated cells with a single 1 h pulse of 100 ng/ml of IFN- $\gamma$ . We found that STAT1-tagRFP translocation kinetics were similar to that of the continuous treatment ([Figures 1A–C](#)). There were no differences in peak amplitude of the nuclear STAT1-tagRFP, while differences in the AUC and peak timing were <15% ([Figure 1C](#)). To quantify the level of desensitization following a single IFN- $\gamma$  pulse, a second 1 h pulse of 100 ng/ml of IFN- $\gamma$  was applied 6 hours after the end of the first pulse (referred here as 6 h pulsing interval). We found that cells were refractory to the second IFN- $\gamma$  pulse as they exhibited no detectable STAT1 activation ([Figures 1A–C](#)). The lack of STAT1-tagRFP activation was also observed when the pulsing interval was extended to up to 24 h, either in iBMDMs assayed on the microscope for the entire duration of the experiment or only during the second (and third pulse) ([Figure 1D](#)).

Imaging approaches provide insights into response variability. While all cells responded to saturating IFN- $\gamma$  treatment, STAT1-tagRFP trajectories exhibited cell-to-cell variability in terms of the AUC and peak amplitude ([Figure 1C](#)). Notably, both showed significant positive correlations with resting nuclear or cytoplasmic STAT1 levels (at  $t=0$  mins) ([Figures S1B, C](#)). We also found significant correlations between the AUC of the response to 1<sup>st</sup> vs. 2<sup>nd</sup> pulse ( $r=0.6$ ,  $p\text{-val}<0.0001$ ) and AUC of the response to the 2<sup>nd</sup> pulse vs. the nuclear STAT1-tagRFP levels before treatment (at 420 mins, [Figure S1C](#)). This demonstrates that the level of the stimuli-induced STAT1 activation is proportional to the total (and nuclear) resting levels, while the observed variability is likely associated with cell intrinsic differences in STAT1 expression between cells, as demonstrated for other signaling systems (46–48). This is consistent with recent analyses of IFN- $\gamma$  signaling demonstrating that phenotypic variability rather than random noise controls heterogeneity of STAT1 responses (49).

IFN- $\gamma$  regulates hundreds of target genes, which rely on STAT1-dependent transcription (17). To evaluate whether desensitization of STAT1 signaling resulted in functional inhibition of inducible gene expression, population-level qRT-PCR was performed ([Figure 1E](#)). We found that IFN- $\gamma$  upregulated expression across a panel of 6 genes (at 7 h and 10 h following the 1 h pulse of 100 ng/ml of IFN- $\gamma$ ). However,

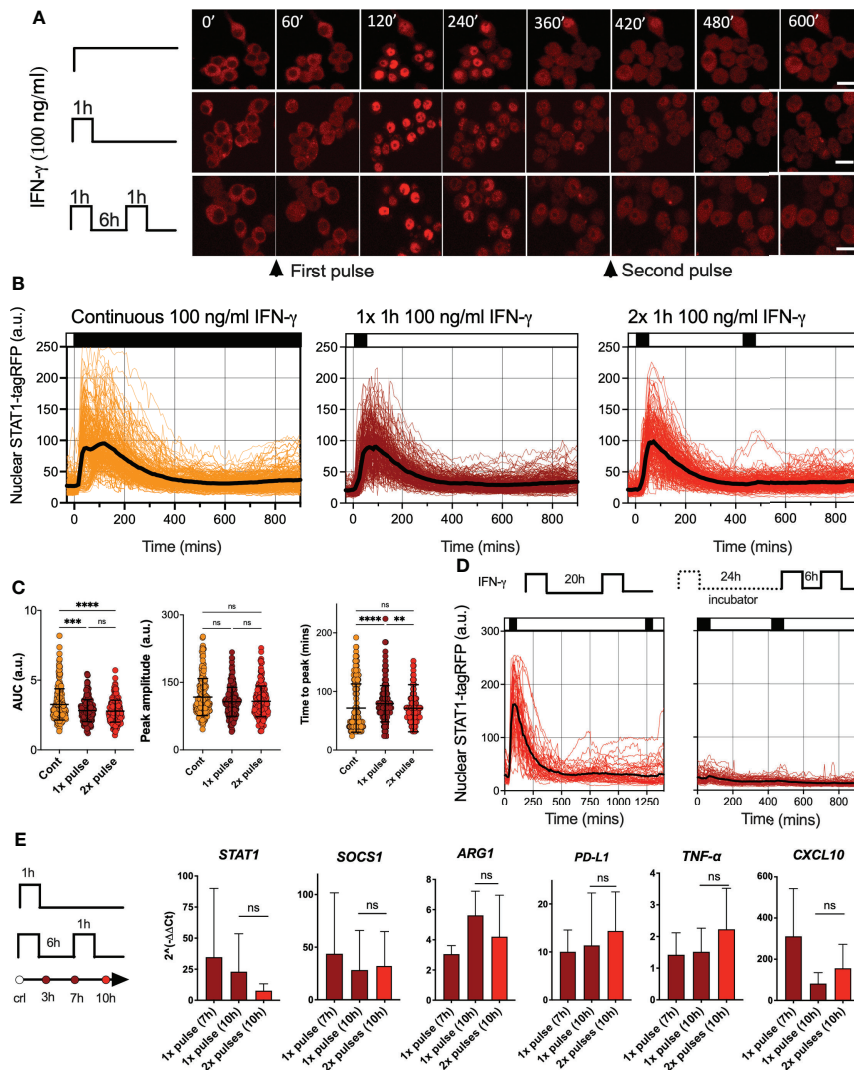


FIGURE 1

IFN- $\gamma$  induces desensitization of STAT1 signaling (A) Representative confocal microscopy images of STAT1-tagRFP iBMDMs cells stimulated with continuous, 1h pulse or two 1h pulses of 100ng/ml of IFN- $\gamma$  at 6h interval. Time stamp in mins, scale bar 10  $\mu$ m. (B) Temporal STAT1-tagRFP trajectories in reporter iBMDMs in response to different IFN- $\gamma$  treatment protocols (as indicated on the graph). Shown are individual nuclear STAT1-tagRFP trajectories (color-coded according to treatment protocol) as well as ensemble average (in black) for 224, 216 and 204 cells for continuous, 1h pulse or two 1h pulses at 6h interval, from three replicates, respectively. STAT1-tagRFP fluorescence shown in arbitrary units (a.u.), time in minutes (mins). (C) Characteristics of single cell nuclear STAT1 trajectories presented in (B) From the left: distributions of AUC (over 10h), peak amplitude, and time to peak under different treatment conditions. Individual cell data depicted with circles (with mean  $\pm$  SD per condition) and color-coded according to treatment protocol. Kruskal-Wallis one-way ANOVA with Dunn's multiple comparisons test was used to assess differences between groups (\*\* $p < 0.01$ , \*\*\* $p < 0.001$ , \*\*\*\* $p < 0.0001$ , ns, not significant). (D) Temporal STAT1-tagRFP trajectories in reporter iBMDMs in response to long interval IFN- $\gamma$  pulsing protocols. Shown are individual nuclear STAT1-tagRFP trajectories as well as ensemble average (in black) for 49 and 67 cells treated with two 1h 100 ng/ml IFN- $\gamma$  pulses at 20h interval (an imaged under the microscope throughout the experiment) or two pulses at 24h interval (and additional pulse 6h later) while maintaining cells in the incubator before the second pulse. STAT1-tagRFP fluorescence shown in arbitrary units (a.u.), time in minutes (mins). Data from two replicates. (E) Fold change of STAT1, SOCS1, ARG1, PD-L1, TNF- $\alpha$  and CXCL10 gene expression response as assessed by qRT-PCR. Wild type iBMDMs stimulated with a 1h pulse of 100ng/ml IFN- $\gamma$ , or two 1h pulses of 100ng/ml IFN- $\gamma$  at 6h interval. Shown is the mean fold change ( $2^{\Delta\Delta Ct}$ ), against unstimulated controls) and SD from three replicates measured at 7 and 10 h after the start of the experiment, respectively. Non-parametric Mann Whitney test was used to determine statistical significance between conditions (ns, not significant,  $p > 0.05$ ).

consistent with desensitization, the expression of *Stat1*, *Socs1*, *Arg1*, *Cxcl10*, *Tnf- $\alpha$*  and *Cd274* mRNA following the second 1 h pulse of 100 ng/ml of IFN- $\gamma$  at the 6 h interval showed no further induction in comparison to cells stimulated with a single pulse, measured at 10 h from the beginning of the experiment. Overall, these analyses demonstrate that a pulse IFN- $\gamma$  stimulation induces a long-lasting desensitization of STAT1 signaling and gene expression responses, which renders cells refractory to stimulus upon re-exposure.

## Desensitization of STAT1 signaling depends on dose and timing of IFN- $\gamma$

To further investigate the regulation of desensitization, reporter iBMDMs were treated with two pulses of IFN- $\gamma$  at 6 h intervals, such that the concentration of the first pulse was varied (100, 10, 5 and 1 ng/ml), while the concentration of the second pulse was constant at 100 ng/ml (Figure 2A). In response to the varied concentration of the first pulse, STAT1-tagRFP activity showed a dose-dependency, with each consecutive nuclear peak amplitude (P1) being significantly higher as the dose increased (Figure 2B). The response to the second 100 ng/ml pulse was also varied, but we found that it was determined by the amplitude of the first response, i.e., the higher the initial response the lower the response to the 2<sup>nd</sup> pulse. This was marked by significant increases in the peak nuclear STAT1-tagRFP amplitude (P2) as the dose of the first pulse decreased (except for the 100-100 pulsing regime where only few cells exhibited detectable responses to the second pulse). The responses to the first and second pulse measured as peak nuclear STAT1-tagRFP showed significant positive correlations across doses (of at least  $r=0.4$ ,  $p<0.0001$ , Figure 2B), suggesting an intrinsic ability of some cells to respond more robustly to both pulses. We found that the saturated 100 ng/ml dose (in the first pulse) produced a significantly higher nuclear STAT1-tagRFP response in terms of the AUC, when compared to other pulsing protocols over the 840 mins duration of the experiment (Figure 2C). However, when stimulated with non-saturating doses (in the first pulse), cells exhibit the same AUC irrespectively of the concentration of the first pulse. This suggest that the overall temporal STAT1 response to multiple IFN- $\gamma$  inputs is inherently restricted.

We hypothesized that the desensitization is associated with availability of signaling complexes, for example through a depletion of IFN $\gamma$ R receptors and/or JAK signaling complexes from a total pool available for activation (50, 51). In this case, in response to sub-saturating doses (which would engage fewer signaling molecules) cells are expected to maintain their responsiveness. In contrast, our data show that even a low dose 1 ng/ml IFN- $\gamma$  resulted in reduced responses to a subsequent saturated treatment (Figure 2A). To test this further, reporter iBMDMs were treated with two pulses of IFN- $\gamma$  at 6 h interval, such that the concentration of the first pulse was 1 ng/ml, while the concentration of the second pulse was varied (100,

10, 5 and 1 ng/ml) (Figure 3A). We found detectable STAT1 responses to the first and second pulses across all IFN- $\gamma$  concentrations (Figure 3B). In response to 1 ng/ml, the peak nuclear STAT1-tagRFP amplitude in the second pulse was significantly lower to that of the first pulse, consistent with pathway desensitization (Figure 3B). Similarly, the responses to 5 ng/ml and 10 ng/ml pulses were significantly lower than responses induced by the same dose applied in the first pulse (Figure 3C). Therefore, these data suggest a model where the first pulse induces a dose-dependent 'signal threshold', which subsequently reduces STAT1 responsiveness upon re-exposure to stimulus.

Finally, we examined whether the level of desensitization was related to the timing of IFN- $\gamma$  stimulation. We subjected reporter iBMDMs to three pulses of IFN- $\gamma$  at 3 h interval, using matched but different sub-saturating doses (10, 5 and 1 ng/ml) per condition (Figure 3D). We found that there was no or very little activation in response to the second and third pulse at 3 h interval, regardless of the dose (Figure 3D). This demonstrates that desensitization is induced rapidly, before the initial STAT1 response subsides (e.g., in the timescale of 3 h) such that the system is refractory to the same dose (upon re-exposure).

Overall, these data demonstrate that STAT1 desensitization is dose-dependent, where the level of activation to a stimulation depends on the past (first) IFN- $\gamma$  dose, revealing a 'signal memory' within the JAK-STAT network. This is consistent with a mechanism, where an initial stimulation sets a 'signal threshold', which subsequent treatment must overcome, consequently resulting in reduced responses upon re-exposure. Our data suggest that to elicit a similar signaling response, the dose of IFN- $\gamma$  upon re-exposure must be higher than that of the initial treatment.

## Type II and type I interferons differentially control JAK-STAT pathway desensitization

Type II (IFN- $\gamma$ ) and type I IFNs cytokine family (including IFN- $\alpha$  and IFN- $\beta$ ) play distinct functions in the immune response (17). Both interferons use unique signaling components of the Janus Kinase (JAK)-STAT signaling pathway with a notable exception of signaling adapters, where IFN- $\gamma$  signals *via* JAK1 and JAK2 adaptor proteins, while IFN- $\alpha$  and IFN- $\beta$  engage IFNAR complex and JAK1 and Tyrosine Kinase 2 (TYK2) (13). To provide more insights into control of the JAK-STAT pathway desensitization, we assayed responses to pulsatile type I and II interferon stimulation. First, we subjected reporter iBMDMs to pulsatile treatment of the combined 50 ng/ml of IFN- $\alpha$  and 50 ng/ml of IFN- $\beta$ 1 (referred hereafter to 100 ng/ml IFN- $\alpha/\beta$ 1). We found that a 1 h pulse induces a single nuclear translocation of STAT1-tagRFP, and the system was refractory to a subsequent pulse of IFN- $\alpha/\beta$ 1 at 6 h interval as indicated by single cell trajectories and their AUC (Figures 4A, B). This confirms that type I interferons induce complete self-

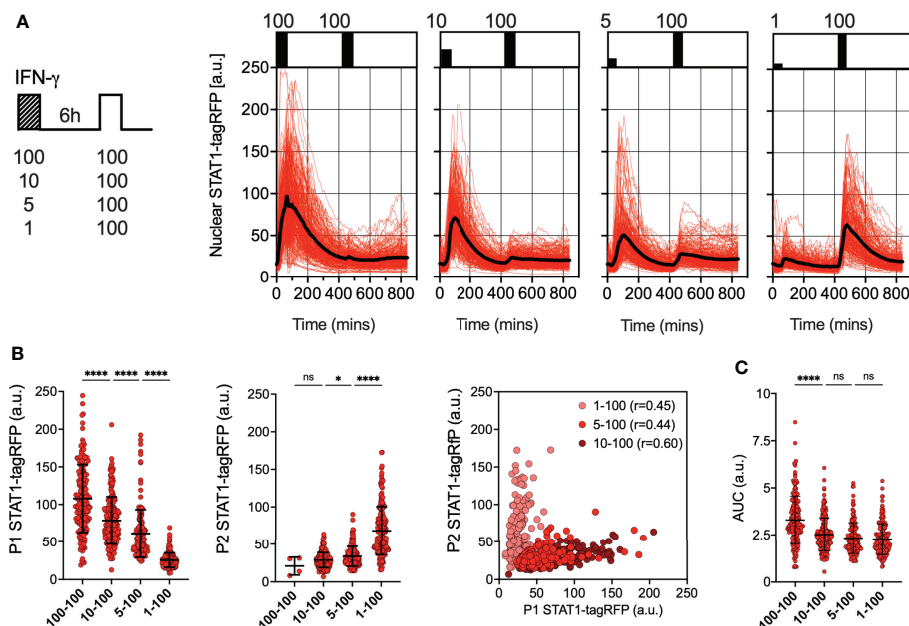


FIGURE 2

Desensitization of STAT1 signaling is dose-dependent (A) Single cell analyses of STAT1 responses to IFN- $\gamma$  pulses of different concentration. Left: Schematic diagram of the IFN- $\gamma$  treatment protocol; reporter iBMDMs stimulated with two 1h pulses of IFN- $\gamma$  at 6h interval. Dose of the first pulse varied (100, 10, 5 and 1ng/ml) while the dose of the second pulse was kept constant at 100 ng/ml. Right: Temporal STAT1-tagRFP trajectories in reporter iBMDMs in response to different IFN- $\gamma$  treatment protocols (as indicated on the graph). Shown are individual nuclear STAT1-tagRFP trajectories as well as ensemble average (in black) for 192, 210, 196 and 204 cells for 100, 10, 5 and 1 ng/ml first dose, respectively, based on duplicated experiments. STAT1-tagRFP fluorescence shown in arbitrary units (a.u.), time in minutes (mins). (B) Characteristics of single cell nuclear STAT1 trajectories presented in (A) From the left: distributions of peak nuclear STAT1-tagRFP amplitude in response to first (P1) and second pulse (P2). Individual cell data depicted with circles (with mean  $\pm$  SD per condition) and color-coded according to treatment protocol. Kruskal-Wallis one-way ANOVA with Dunn's multiple comparisons test was used to assess differences between groups (\* $p$  < 0.05, \*\*\*\* $p$  < 0.0001, ns, not significant). Right: Correlation between peak nuclear amplitudes with corresponding Spearman's correlation coefficients, cooler coded according to treatment protocol. (C) Distributions of the overall STAT1-tagRFP AUC (over 14h) across treatment protocols. Individual cell data depicted with circles (with mean  $\pm$  SD per condition) and color-coded according to treatment protocol. Kruskal-Wallis one-way ANOVA with Dunn's multiple comparisons test was used to assess differences between groups \*\*\*\* $p$  < 0.0001, ns, not significant).

desensitization of STAT1 signaling in macrophages (36). We then treated cells with 1 h pulses of IFN- $\alpha/\beta$ 1 and IFN- $\gamma$  (at 6 h interval) in different orders (Figure 4C). We found that after IFN- $\alpha/\beta$ 1 treatment cells were able to respond to second pulse of IFN- $\gamma$ , however, when we reversed the order of stimulation cells became refractory to IFN- $\alpha/\beta$ 1. This is consistent with complete cross-desensitization of JAK-STAT signaling by IFN- $\gamma$  and partial desensitization by IFN- $\alpha/\beta$ 1. Counterintuitively, the overall nuclear STAT1-tagRFP AUC was higher in cells treated first with IFN- $\gamma$  than those first treated with IFN- $\alpha/\beta$ 1 (Figure 4D). This resulted from a reduced response amplitude to the IFN- $\alpha/\beta$ 1 stimulation in the first pulse, in comparison to IFN- $\gamma$ , while the timing of responses remained the same (Figure 4E). In cells treated with pulse of IFN- $\alpha/\beta$ 1 followed by pulse of IFN- $\gamma$ , we found a significant positive correlation ( $r=0.34$ ) between the 1<sup>st</sup> and 2<sup>nd</sup> peak nuclear STAT1 AUC suggesting that individual cells exhibited similar sensitivity to both stimuli (Figure 4F). These data demonstrate that IFN- $\gamma$  and

IFN- $\alpha/\beta$ 1 differentially regulate JAK-STAT pathway desensitization, suggesting prioritization of IFN- $\gamma$  signaling over IFN- $\alpha/\beta$ 1 through regulatory crosstalk

## Desensitization is regulated post-transcriptionally via STAT1 phosphorylation

Having observed JAK-STAT pathway desensitization we wanted to understand the underlying molecular mechanisms. Our imaging data suggested that the phenomenon is not driven by lack of availability of signaling complexes upon re-exposure (Figure 3A), which we wanted to test experimentally. IFN- $\gamma$  exerts its biological function through binding to the IFN $\gamma$ R1 receptor dimer, which subsequently recruits two chains of IFN $\gamma$ R2 to form the signaling complex (14). IFN- $\gamma$  uptake initiates internalization of the IFN $\gamma$ R complex, thus the

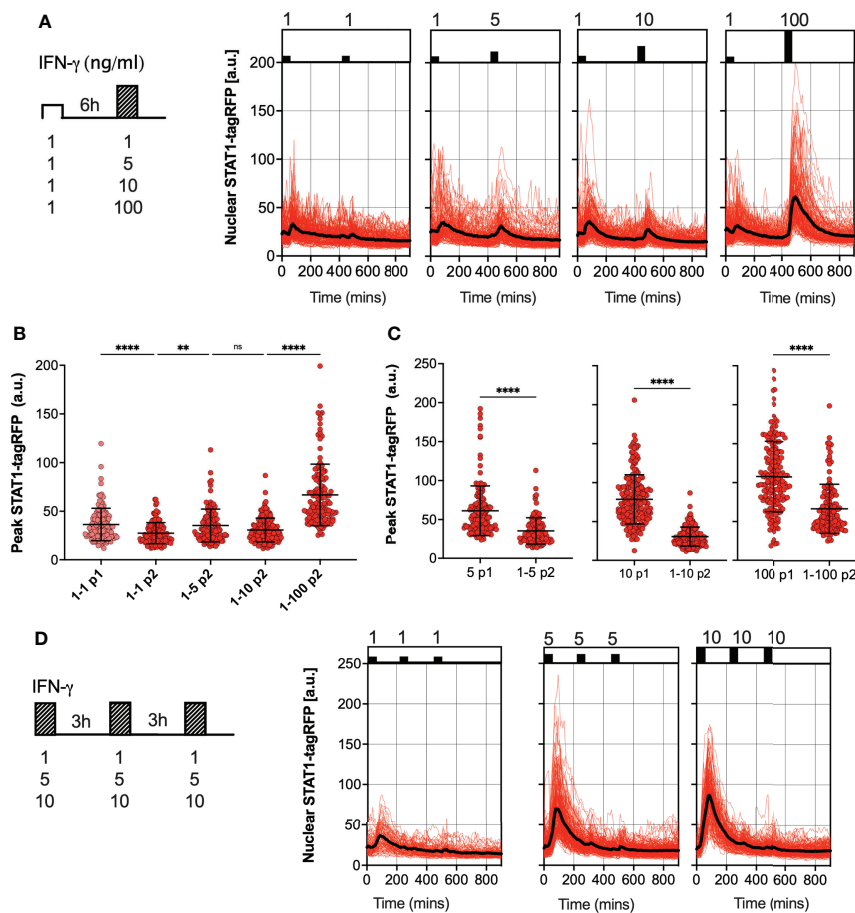


FIGURE 3

Sub-saturating and high frequency IFN- $\gamma$  pulses increase signal threshold (A) Single cell analyses of STAT1 responses to IFN- $\gamma$  pulses of different concentration. Left: Schematic diagram of the IFN- $\gamma$  treatment protocol; reporter iBMDMs stimulated with two 1h pulses of IFN- $\gamma$  at 6h interval. Dose of the first pulse kept at 1ng/ml, dose of the second pulse varied (100, 10, 5 and 1ng/ml). Right: Temporal STAT1-tagRFP trajectories in reporter iBMDMs in response to different IFN- $\gamma$  treatment protocols (as indicated on the graph). Shown are individual nuclear STAT1-tagRFP trajectories as well as ensemble average (in black) for 148, 116, 160 and 132 cells for 1, 5, 10 and 100 ng/ml second dose, respectively, based on duplicated experiments. STAT1-tagRFP fluorescence shown in arbitrary units (a.u.), time in minutes (mins). (B) Characteristics of single cell nuclear STAT1 trajectories presented in (A) Show is peak nuclear STAT1-tagRFP amplitude in response to first (P1) and second pulse (P2). Individual cell data depicted with circles (with mean  $\pm$  SD per condition) and color-coded according to treatment protocol. Kruskal-Wallis one-way ANOVA with Dunn's multiple comparisons test was used to assess differences between groups (\*\* $p < 0.01$ , and \*\*\*\* $p < 0.0001$ , ns, not significant). (C) Low dose stimulation induces STAT1 desensitization. Shown are the peak nuclear STAT1-tagRFP amplitudes in response to second pulse (P2) across doses (5,10 and 100 ng/ml), when stimulated with 1 ng/ml in the first pulse (data from P1) and second pulse (P2). Individual cell data depicted with circles (with mean  $\pm$  SD per condition) and color-coded according to treatment protocol. Mann-Whitney pairwise comparisons test was used to assess differences between groups (\*\*\*\* $p < 0.0001$ ). (D) Single cell analyses of STAT1 responses to IFN- $\gamma$  pulses at 3 h interval. Left: Schematic diagram of the IFN- $\gamma$  treatment protocol; reporter iBMDMs stimulated with two 1 h pulses of IFN- $\gamma$  at 3 h interval. First and second pulse dose matched, but varied across treatments (1, 5 and 10 ng/ml). Right: Temporal STAT1-tagRFP trajectories in reporter iBMDMs in response to different IFN- $\gamma$  treatment protocols (as indicated on the graph). Shown are individual nuclear STAT1-tagRFP trajectories as well as ensemble average (in black) for 74, 163 and 138 cells for 1, 5 and 10 ng/ml treatment, respectively, based on duplicated experiments. STAT1-tagRFP fluorescence shown in arbitrary units (a.u.), time in minutes (mins).

reduced cell surface expression of the receptor may therefore act as mechanism to limit the level of response (51). The quantification of cell-surface receptor expression showed that untreated (control) iBMDMs express a basal level of IFN $\gamma$ R1, which was substantially reduced by continuous 100 ng/ml IFN- $\gamma$  treatment (Figure S2). 1 h pulse of 100 ng/ml IFN- $\gamma$  decreased the expression of IFN $\gamma$ R1 compared to control cells, but most of

the receptor was still present on the cell surface. As an additional control, we showed that IFN $\gamma$ R1 expression was not affected by the 100 ng/ml of IFN- $\alpha$ / $\beta$ 1, which specifically bind to its own cognate receptor (13). In terms of IFN $\gamma$ R2 expression, the continuous treatment with IFN- $\gamma$  substantially reduced IFN $\gamma$ R2 expression at 6h, but neither IFN- $\gamma$  nor IFN- $\alpha$ / $\beta$ 1 pulses had a substantial impact on the level of expression.



Therefore, to globally evaluate the role of transcriptional feedback we used RNA polymerase inhibitor Actinomycin D (ActD) (52) to prevent *de novo* mRNA synthesis and subsequently monitor STAT1 responses *via* microscopy. In these experiments, reporter iBMDMs were simulated with two 1 h 100 ng/ml IFN- $\gamma$  pulses at 6 h interval, while treated with ActD either for 2 h before the first pulse or between the two pulses (Figure 5A). We found that following the ActD treatment STAT1-tagRFP showed a higher level of activity in comparison to control cells, as evident by more prolonged nuclear localization. Importantly, while ActD treatment did not alter the amplitude of the STAT1 response to the first pulse (Figure 5B), there were no apparent changes to cell responsiveness as we observed a very limited response to the second pulse. IFN-mediated STAT1 nuclear export is controlled *via* Crm1-dependent mechanisms (53, 54), which in some context involve transcriptional regulation of Crm1 level (55). As such, our data are consistent with this, but demonstrate that *de novo* transcription is not causing desensitization following IFN- $\gamma$  stimulation.

Phosphorylation of STAT1 is necessary for cytokine-induced nuclear translocation and regulation of target gene expression (14). Therefore, using Western blotting, we examined phosphorylation patterns of STAT1 tyrosine 701 (Y701), a marker of STAT1 activation in response to pulsatile treatment (Figure 5C; Figures S3B–D for quantification). Whereas phosphorylated STAT1 (Y701) was not detected in untreated wild type iBMDMs, *de novo* phosphorylation of STAT1 was highly induced upon 10 mins stimulation with 100 ng/ml of IFN- $\gamma$ . Phosphorylated STAT1 were also detected in cells treated with a 1 h pulse of 100 ng/ml IFN- $\gamma$  when examined after 4 h. At 7 and 10 h following the start of the experiment, the STAT1 (Y701) phosphorylation was still maintained, albeit at a lower level (especially at the 10 h time-point). We found an increase of the phosphorylated STAT1 at 10 mins after second IFN- $\gamma$  pulse (which in part might be due to the upregulated STAT1 protein levels). However, at 4 h after the second pulse (10h from the start of the experiment) the phosphorylation was substantially reduced, and in fact lower than the corresponding response to a single 100 ng/ml IFN- $\gamma$  pulse (Figure 5C and Figure S3C). As a control we showed that a second pulse of interleukin 4 (IL-4) abolished STAT1 phosphorylation at 10 h. Overall, this data suggested that although STAT1 may be phosphorylated in a response to second IFN- $\gamma$  pulse, it undergoes a rapid de-phosphorylation, which coincides with lack of nuclear translocation in live-cell microscopy data.

## PTP feedback model of JAK-STAT signaling recapitulates IFN-mediated responses

Our data demonstrates that IFN stimulation results in activation of a post-transcriptional negative feedback, which attenuates STAT1 activation upon re-exposure. This is consistent with action of number of protein tyrosine phosphatases, which are known to inhibit STAT activation

(30). In particular, Tc-PTP (T-cell protein tyrosine phosphatase encoded by PTPN2 gene) was previously found to control STAT1 desensitization in response to pulsatile type I and II interferon stimulation (36, 56). To quantitatively investigate the potential mechanisms involved in the control of desensitization we extended our previous model of JAK-STAT signaling (29) and incorporated new negative feedback due to a putative tyrosine phosphatase PTP (see Figure 6A for a schematic representation of the mathematical model). The second, positive feedback involved regulation of STAT1 expression, through STAT1-mediated activation of Interferon Regulatory Factor 1 (IRF1) (33, 57). In the model, we assume that IFN- $\gamma$  and IFN- $\alpha/\beta$  bind their cognate receptors, forming an active receptor complexes, which phosphorylate STAT1 and STAT2 in the cytoplasm (18). Phosphorylated STATs (pSTAT1 and pSTAT2) undergo homo- and hetero- dimerization. While the responses to IFN- $\gamma$  exclusively involve the former, IFN- $\alpha/\beta$  also activates STAT1-STAT2-IRF9 (ISG3) complex (29). The mathematical model representation consisted of 37 differential equations and 65 parameters to recapitulate the ‘average’ behaviour of the JAK-STAT signaling system with a subset of parameters fitted *de novo* (see Tables S2 to S5 for list of variables, ordinary differential equations, fitted parameters and initial conditions). The model was able to accurately recapitulate single-cell STAT1 translocation data for continuous and pulsatile IFN- $\gamma$  and IFN- $\alpha/\beta$  treatment (Figures 6B–D) as well as kinetics of STAT1 mRNA and protein production (Figures S4A–C). However, it did not recapitulate ActD-mediated modulation of STAT1 export (Figure 5A) due to insufficient mechanistic insight.

The main regulatory feedback in the model loop involves activation of PTP *via* the active receptor (58). Following previous work, we assumed that activated PTP both inhibits the receptor complex (59) as well as directly de-phosphorylate STATs (60) leading to dissociation of STAT complexes and nuclear export (30). *In silico* PTP knockout resulted in complete sensitization to type I and type II interferons, such that cells exhibited full STAT1 activation in response both IFN- $\gamma$  or IFN- $\alpha/\beta$  pulses at 6 h interval (Figure S4D). While in general the desensitization relied additively on both feedback targets, they differently affected IFN- $\gamma$  and IFN- $\alpha/\beta$  signaling. In the model it was due to differences in the active receptor half-life, 110 mins for IFN- $\gamma$  vs 60 mins IFN- $\alpha/\beta$  reported by the previous work (61–63). Since the active receptor complexes signal until degraded or inhibited (59, 64), the slow degradation of IFN- $\gamma$  complexes is compensated in the model by PTP-mediated inhibition to prevent prolonged nuclear STAT1 accumulation. Consequently, PTP-mediated de-phosphorylation of STAT1 affected IFN- $\gamma$  responses more than the inhibition of the receptor complex by controlling STAT1 nuclear localization (and recovery to the steady-state, Figure S4D). In contrast, IFN- $\alpha/\beta$ -mediated signaling was predominantly affected by the inhibition of the receptor complex than PTP-mediated de-

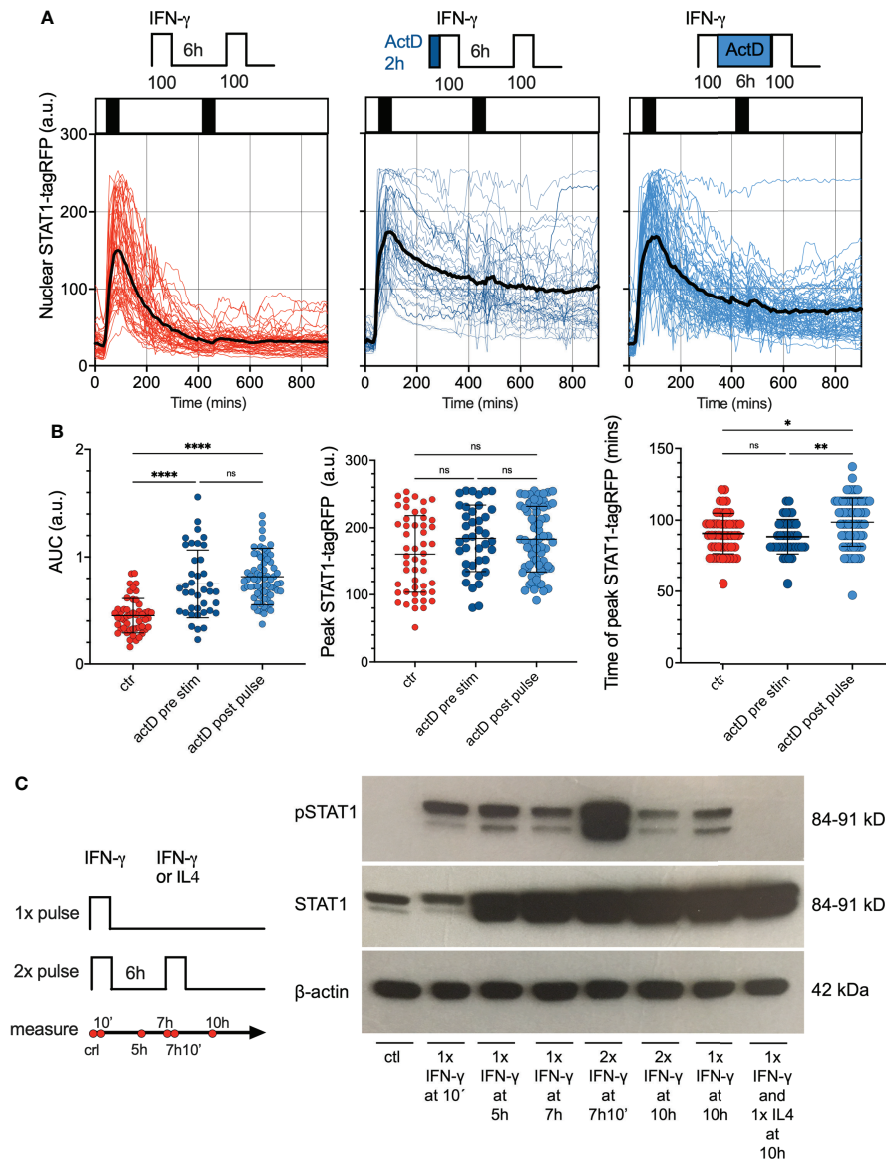


**FIGURE 5**

Feedback control of STAT1 desensitization. **(A)** Single cell analyses of STAT1 responses in presence of transcriptional inhibitors. Reporter cells stimulated with two 1 h pulses of 100 ng/ml IFN- $\gamma$  (control, left), pre-treated with 5  $\mu$ g/ml of ActD for 2h before the first pulse (middle) or treated with 5  $\mu$ g/ml of ActD between the first and second pulse (right). Shown are individual nuclear STAT1-tagRFP trajectories (color-coded according to treatment protocol) as well as ensemble average (in black) for 50, 39 and 68 cells for control, ActD pre-treatment and ActD treatment between pulses, from two replicates, respectively. STAT1-tagRFP fluorescence shown in arbitrary units (a.u.), time in minutes (mins). **(B)** Characteristics of single cell STAT1 trajectories presented in **(B)** From the left: distributions of the overall AUC, peak amplitude (in response to first pulse), and time to peak (in response to first pulse) under different treatment conditions. Individual cell data depicted with circles (with mean  $\pm$  SD per condition) and color-coded according to treatment protocol. Kruskal-Wallis one-way ANOVA with Dunn's multiple comparisons test was used to assess differences between groups (\* $p < 0.05$ , \*\* $p < 0.01$ , \*\*\*\* $p < 0.0001$ , ns, not significant). **(C)** Phosphorylation pattern of STAT1 (Y701) during pulsatile treatment of iBMDMs. Wild type iBMDMs either untreated (ctrl) or stimulated with one or two 1h pulses of 100 ng/ml IFN- $\gamma$  at 6h interval. In addition, 100 ng/ml of IL4 was used in the second pulse applied at 6h interval following a pulse of IFN- $\gamma$ . Samples analyzed at 10 mins, 5h, 7h, 7h and 10mins, and 10h after the start of the experiment. B-actin included as a loading control. Schematic diagram represents pulsing protocol and measurement time-points (in red circles). Molecular weight (MW) is shown in kilo Dalton (kDa). Data are representative of two replicates.

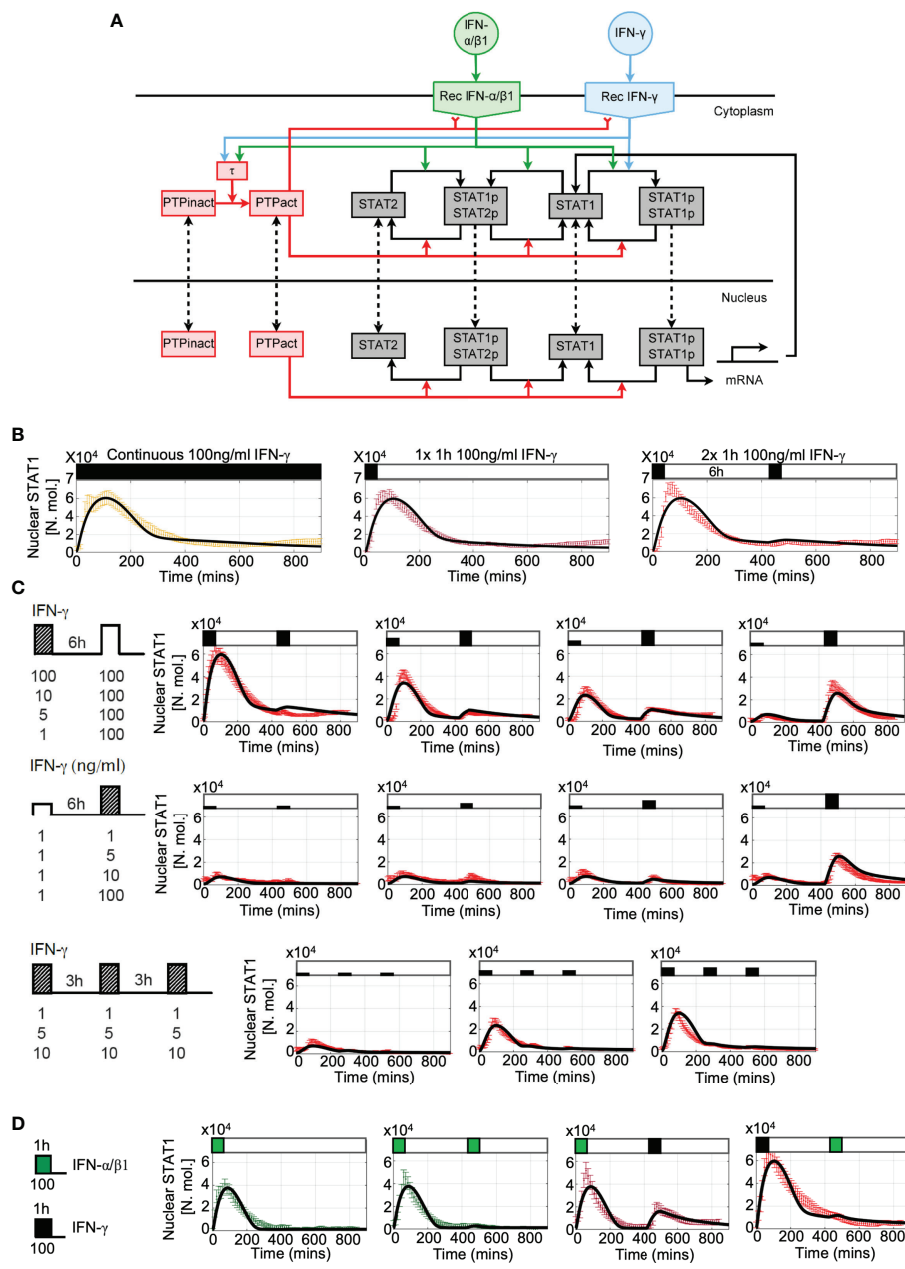


FIGURE 6

Mathematical model of JAK-STAT pathway desensitization (A) Schematic representation of the JAK-STAT signaling network. IFN stimulation results in receptor binding, activation, and internalization, leading to STAT1 phosphorylation and translocation to the nucleus. Stimuli-induced putative tyrosine kinase PTP inhibits receptor activity and STAT1 phosphorylation. (B) Mathematical model recapitulates IFN- $\gamma$ -induced desensitization. Shown is the simulated nuclear STAT1 in number of molecules (in black) and scaled experimental data (from Figure 1B, in color, shown as mean with 99% confidence intervals). Cells treated with 100 ng/ml of IFN- $\gamma$  either as continuous (left), one 1h pulse (middle) and two 1 h pulses at 6 h interval. (C) Model recapitulates responses to different doses and timing of IFN- $\gamma$  stimulation. Shown are simulated nuclear STAT1 expressed in number of molecules (in black) and scaled experimental data (mean with 99% confidence intervals in red) across different stimulation protocols (as highlighted with schematic diagrams). Top: Two 1 h pulses of IFN- $\gamma$  at 6h interval as in Figure 2A, Middle: low dose priming as in Figure 3A. Bottom: 1 h pulses of IFN- $\gamma$  at 3 h interval as in Figure 3C. (D) Model recapitulates IFN- $\gamma$  and IFN- $\alpha/\beta$  cross-talk. Simulated nuclear STAT1 expressed in number of molecules (in black) and scaled experimental data (mean with 99% confidence intervals). Cells either treated with 1h pulse of IFN- $\alpha/\beta$ , two pulses of IFN- $\alpha/\beta$  at 6 h interval, or combination of 1 h pulses of IFN- $\gamma$  and IFN- $\alpha/\beta$  (as in Figure 4A).

phosphorylation of STAT1, since the effect of the latter on the nuclear accumulation was reduced due to faster receptor complex degradation. Finally, analysis of the model demonstrates that desensitization was not affected by the level of STAT1 expression, such that a substantial build-up of STAT1 protein had a minor effect on responses to IFN- $\gamma$  stimulation at 24 h pulsing interval (Figure S4C).

## Pathway desensitization renders cells with signal memory of interferon stimulation

Having fitted the new JAK-STAT model to the microscopy data we wanted to systematically investigate the control of pathway desensitization. We assume that in resting cells PTP exists in the inactive form, which upon IFN stimulation undergoes activation *via* the receptor complex. In response to 100 ng/ml IFN- $\gamma$  pulse stimulation, PTP activity exhibited saturated non-linear kinetics, characterized by rapid increase to its maximal level at around 6 h (Figure 7A). At lower IFN- $\gamma$  concentrations, PTP activation was delayed and reduced over the 800 mins time course, however even the lowest 1 ng/ml dose was able to induce considerable PTP activity. Such a model fit was a consequence of imaging data which demonstrate that 1 ng/ml pulse caused ~50% reduction in STAT1 response amplitude upon exposure to saturated IFN- $\gamma$  concentration (Figure 6C).

To better understand the relationship between dose of the stimulus, PTP activity and STAT1 translocation kinetics we simulated responses to two IFN- $\gamma$  pulses for ~5000 different combinations of doses across 100 ng/ml range (with 1 ng/ml step, Figure 7B). We find that the different (dose-dependent) levels of PTP activity quantitatively determine whether the system responds to stimulus (at the time of the second pulse) and if it does so, the amplitude of the response. In general, to elicit any signaling response upon re-exposure (defined as the >5% of the amplitude of the single 100 ng/ml IFN- $\gamma$  pulse) the dose of the 2<sup>nd</sup> pulse must be substantially higher than the dose of the 1<sup>st</sup> pulse (Figure 7B, middle). At 3 h pulsing interval, to achieve 5% response the dose of the second pulse must be ~3-times larger than the dose of the 1<sup>st</sup> pulse, while ~8- and ~30-times larger concentrations are required to achieve 20% and 50% response, respectively. As the level of PTP activity increases with time, the sensitivity to second pulse is reduced, such that at 6 h, the dose of the second pulse must be at least ~35 times higher than the dose of the first pulse to elicit a 20% response, while 50% response can only be achieved following a 1 ng/ml stimulation. Notably, the observed relationships between the doses are linear (apart for the 5% response for the 6 h pulsing interval), while the same level of response to the 2<sup>nd</sup> pulse can be achieved by combinations of IFN- $\gamma$  concentration, suggesting that the system may effectively respond to the relative fold changes of input concentration. Subsequently, we investigated

the overall sensitivity of STAT1 response to IFN- $\gamma$  pulses (Figure 7B, right). We found that the AUC of the nuclear STAT1 in response to two pulses (at 3 and 6 h pulsing intervals) was inherently restricted; that is the overall responses was not higher than the AUC of the single 1 h 100 ng/ml pulse (calculated over the same time interval). For concentrations above >16 ng/ml of IFN- $\gamma$  at 6 h pulsing intervals (and >50 ng/ml for 3 h) any further stimulation had a minor effect on the overall response (i.e., the relative AUC changes <10% with respect to the 2<sup>nd</sup> pulse dose), but the system exhibited sensitivity the 1<sup>st</sup> pulse dose. In turn, at lower concentration (<2.5 ng/ml for 6 h and <12 ng/ml for 3 h intervals) the overall AUC exhibited increased sensitivity to the 2<sup>nd</sup> pulse (i.e., >20% AUC change), in particular high IFN- $\gamma$  concentrations. This demonstrates that while maintaining the overall dose-dependency, the PTP feedback restricts the temporal JAK-STAT signaling response to that of a single transient and saturated IFN- $\gamma$  input.

Finally, we investigated the role of the PTP feedback in the crosstalk between IFN- $\gamma$  and IFN- $\alpha/\beta$ 1 pulses. In agreement with experimental data, the mathematical model demonstrated that IFN- $\alpha/\beta$ 1 stimulation induced a lower STAT1 translocation (Figure 4E), which resulted in a lower PTP activity, in comparison to matching doses of IFN- $\gamma$  (Figure S5A). Consequently, PTP activity induced *via* IFN- $\alpha/\beta$ 1 was not sufficient to inhibit responses upon to IFN- $\gamma$  stimulation. We found that ~1.5-fold change in IFN- $\gamma$  dose (comparing to that of IFN- $\alpha/\beta$ 1) was required to elicit a 5% response and ~4-fold change for a 20% of the response upon re-exposure (Figure S5B). Consequently, the overall AUC of nuclear STAT1 exhibited more sensitivity to IFN- $\gamma$  (defined as 20% AUC change) than to IFN- $\alpha/\beta$ 1, in cells stimulated with IFN- $\alpha/\beta$ 1 in the first pulse. In turn, the level IFN- $\gamma$ -induced STAT1 activation was higher, and consequently higher PTP levels almost completely inhibited responses to subsequent IFN- $\alpha/\beta$ 1 stimulation, resulting in complete desensitization. Overall, these analyses demonstrate that the PTP feedback renders cells with signal memory by responding to the relative fold changes of the IFN concentration and discriminate different temporal patterns of type I and type II interferon stimulation.

## Discussion

Here we provide a new quantitative understanding of JAK-STAT signaling in response to temporal type I and type II IFNs in innate immune macrophages. Using live-cell microscopy to follow intracellular localization of a constitutively expressed fluorescent STAT1 fusion we demonstrate that responses to interferon stimulation are tightly controlled through the desensitization of the JAK-STAT pathway. We demonstrate that a brief 1 h stimulation with saturating concentration of IFN- $\gamma$  elicit quantitatively similar response to that of continuous



work has shown that Tc-PTP feedback controls desensitization to IFN- $\beta$  and IFN- $\gamma$  stimulation (36). Primary human fibroblast exhibited partial desensitization to IFN- $\beta$  after 16 h IFN- $\beta$  treatment as well as to subsequent IFN- $\gamma$  stimulation (at doses <5 ng/ml applied 6 h after initial stimulation) and the attenuation of STAT1 phosphorylation was present in wild type, but not Tc-PTP knockout cells (36). Based on this knowledge we extended our previous mathematical model of IFN- $\beta$ -mediated JAK-STAT signaling system (29) to incorporate a putative PTP feedback and recapitulate our data imaging data on the dose, timing and type of interferon stimulation. The mathematical model likely captures the combined effect of multiple PTPs, but specifically suggests that neither the ability of PTP to block receptor complex nor dephosphorylate STAT1 is sufficient alone to recapitulate observed responses. Surprisingly little is known about regulation of Tc-PTP by IFNs, but recent work demonstrates a direct molecular interaction between a cognate receptor (integrin  $1\alpha$  in the context of cell adhesion) activates Tc-PTP by disrupting the autoinhibitory C-terminal tail of the kinase (58). Further work is required to understand the kinetics of Tc-PTP activity, which we predict lasts beyond the internalized receptor half-life (>24h) as well as to understand potential contributions of other PTPs and in fact other STAT molecules in this process. In the broader context, the quantitative understanding of PTP regulation might provide important insights into control of IFN signaling during immune responses as well as carcinogenesis (65).

Desensitization is a key mechanism that prevents prolonged out-of-control activity to chronic stimulation and/or limit responses upon re-exposure to the same stimulus, for example in the toll-like receptor system (34, 35). Our quantitative imaging data and mathematical modelling demonstrate that through pathway desensitization, the overall JAK-STAT response is restricted, such in response to repeated cues cells cannot produce more activity than to a single 1 h pulse with a saturated IFN- $\gamma$  concentration. Stimulation with sub-saturating IFN- $\gamma$  concentrations resulted in partial STAT1 desensitization, through a dose- and stimulus- dependent negative feedback, and consequently the system's responses upon re-exposure depended on the dose of the initial stimulation and its timing. We found that to elicit a signaling response upon re-exposure, the concentration of IFN- $\gamma$  at 3 and 6 h must be several folds larger than that of the initial stimulation. This effectively means that the JAK-STAT system becomes refractory following stimulation with medium and high IFN- $\gamma$  doses but retains reduced sensitivity to lower concentrations (<10 ng/ml). These analyses predict that through post-transcriptional PTP feedback, desensitization of JAK-STAT signaling renders cells with signal memory by responding to relative fold changes in IFN concentration. In comparison, the NF- $\kappa$ B system can detect absolute increases in cytokine concentration during relatively short (<2h) time intervals (11). Other systems use receptor availability to detect temporal changes in stimulus, for

example, relative (fold) changes in early growth response (EGR) protein concentration (66). Interestingly, we demonstrate that PTP feedback may also distinguish different patterns of type I and II interferon stimulation, such that cells refractory to IFN- $\alpha/\beta$  are sensitive to IFN- $\gamma$ , but not *vice versa*. The type I and II IFNs use unique receptor complexes, thus the overlapping receptor-associated adapters and target STAT activation may result in a functional crosstalk (67). Here we demonstrate that IFN- $\gamma$  and IFN- $\alpha/\beta$  elicit not only different STAT1 translocation profiles, but also different levels of desensitization, where cells exhibit more sensitivity to IFN- $\gamma$  than to IFN- $\alpha/\beta$  (per dose), leading to increased PTP activity in response to IFN- $\gamma$  and subsequently suppression of IFN- $\alpha/\beta$  responses upon re-stimulation. Currently, our model provides a limited insight into differences between IFN- $\gamma$  and IFN- $\alpha/\beta$  signal transduction as we assumed the same rate kinetics except of receptor half-lives (61–63). The model also recapitulates our data which demonstrate that dose-per-dose IFN- $\gamma$  induces a more robust STAT1 response than IFN- $\alpha/\beta$  (Figure 4E). However, it will be important to understand signal specific mechanisms and in particular receptor specificity for different PTPs (30). We suggest that prioritization of IFN- $\gamma$  signaling might reflect different roles during pathogen infection, tissue specificity and timing (14) and reflect specific interactions with pathogens, for example *L. monocytogenes*, where type I and type II interferons induce opposite effects in terms of host susceptibility (68).

Previous work demonstrates the involvement of positive feedback in JAK-STAT signaling; low-dose IFN- $\gamma$  sensitized human PMBCs to IFN- $\alpha$  stimulation through upregulation of JAK-STAT signaling molecules including STATs (33, 57, 69). JAK-STAT pathway desensitization was also shown to depend on the dose of the treatment in hepatocytes, where a 24 h pre-treatment with ~50 pg/ml of IFN- $\alpha$  resulted in increased responsiveness upon re-exposure, while 25 ng/ml IFN- $\alpha$  induced desensitization (25). In this work we only use concentrations of 1 ng/ml and above since we found that lower concentrations do not induce robust STAT1 translocations *via* imaging. However, we expect that the specific effects might reflect differences between (immune vs non-immune) cell types. An important limitation of this study is a use of constitutive STAT1 reporter, which does not allow observing the behaviour of newly synthesized STAT1 proteins. We found that during a 10 h window following IFN- $\gamma$  treatment STAT1 levels may increase ~3 times using population-level immunoblotting (Figure S4A). Our model was fitted to recapitulate *de-novo* STAT1 transcription together with the imaging data, and we showed that inducible STAT1 production had a limited effect on system responses at least up to 24 h after stimulation (Figure S4C). It is however possible that in a longer term (while PTP activity subsides) and the STAT levels increase substantially the JAK-STAT system becomes more sensitive to stimulation. Finally, recent analyses suggest digital activation of STAT1 to IFN- $\gamma$ , where only a fraction of mouse embryonic fibroblasts responding with STAT1

phosphorylation to a particular dose (49). Our data, in agreement with previous work on the NF- $\kappa$ B system, suggest that macrophages exhibit analogue encoding (70, 71), where the dose controls the amplitude of the response, rather than a fraction of responding cells. However, it would be important to understand the variability of key STAT target genes as it may provide the insight into the overall transcriptional control of IFN responses (72). Overall, our analyses demonstrate IFN mediated signaling responses to pulsatile cues are tightly constrained, which we believe facilitates the need within the immune system to control pathological interferon signaling.

## Data availability statement

Tabulated data presented in this study is provided in Table 1. Mathematical model files are available from <https://github.com/ppaszek/Jak-STAT-signal-memory>. Raw imaging data is available on request.

## Author contributions

EK developed cells for imaging, collected, and analyzed data. MK and JS developed mathematical model. JB assisted with cell line development and imaging analyses. DS assisted with imaging analyses. WM, DR, SB, and PP provided supervision and conceptualization. PP with assistance of EK and MK wrote the manuscript. All authors contributed to the article and approved the submitted version.

## Funding

EK was supported by PhD scholarship from the University of Manchester and the Agency for Science, Technology and Research (A\*STAR) in Singapore. This work was also supported by BBSRC (BB/I017976/1 and BB/R007691/1) as well as SUT statutory research funds 02/040/BK\_22/1022 (JS) and 07/040/

BK\_22/1011 (MK). The work has received funding from the European Union Seventh Framework Programme (FP7/2012-2017) under grant agreement no. 305564.

## Acknowledgments

We would like to thank Dr. Kevin Couper for reagents.

## Conflict of interest

The authors declare that the research was conducted in the absence of any commercial or financial relationships that could be construed as a potential conflict of interest.

## Publisher's note

All claims expressed in this article are solely those of the authors and do not necessarily represent those of their affiliated organizations, or those of the publisher, the editors and the reviewers. Any product that may be evaluated in this article, or claim that may be made by its manufacturer, is not guaranteed or endorsed by the publisher.

## Supplementary material

The Supplementary Material for this article can be found online at: <https://www.frontiersin.org/articles/10.3389/fimmu.2022.947213/full#supplementary-material>

### VIDEO 1

Continuous stimulation with 100 ng/ml IFN- $\gamma$ . Confocal microscopy movie of iBMDM cells expressing STAT1-tagRFP (red channel), Venus-STAT6 (yellow channel) and AmCyan-H2B (cyan channel). The time from the start of the experiment is depicted in min. Cells stimulated at time 0 mins.

## References

- Levine JH, Lin Y, Elowitz MB. 'Functional roles of pulsing in genetic circuits'. *Science* (2013) 342:1193–200. doi: 10.1126/science.1239999
- Bhalla US, Iyengar R. 'Emergent properties of networks of biological signaling pathways'. *Science* (1999) 283:381–7. doi: 10.1126/science.283.5400.381
- Novak B, Tyson JJ. 'Design principles of biochemical oscillators'. *Nat Rev Mol Cell Biol* (2008) 9:981–91. doi: 10.1038/nrm2530
- Adelaja A, Taylor B, Sheu KM, Liu Y, Luecke S, Hoffmann A. 'Six distinct NF $\kappa$ B signaling codons convey discrete information to distinguish stimuli and enable appropriate macrophage responses'. *Immunity* (2021) 54:916–30.e7. doi: 10.1016/j.immuni.2021.04.011
- Martin EW, Pacholewska A, Patel H, Dashora H, Sung MH. 'Integrative analysis suggests cell type-specific decoding of NF- $\kappa$ B dynamics'. *Sci Signaling* (2020) 13(620):eaax7195. doi: 10.1126/scisignal.aax7195
- Kellogg RA, Tian C, Etzrodt M, Tay Savaş. 'Cellular decision making by non-integrative processing of TLR inputs'. *Cell Rep* (2017) 19:125–35. doi: 10.1016/j.celrep.2017.03.027
- Adamson A, Boddington C, Downton P, Rowe W, Bagnall J, Lam C, et al. 'Signal transduction controls heterogeneous NF- $\kappa$ B dynamics and target gene expression through cytokine-specific refractory states'. *Nat Commun* (2016) 7:12057. doi: 10.1038/ncomms12057
- DeFelice MM, Clark HR, Hughey JJ, Maayan I, Kudo T, Gutschow MV, et al. 'NF- $\kappa$ B signaling dynamics is controlled by a dose-sensing autoregulatory loop'. *Sci Signaling* (2019) 12(579):eaau3568. doi: 10.1126/scisignal.aau3568
- Ashall L, Horton CA, Nelson DE, Paszek P, Harper CV, Sillitoe K, et al. 'Pulsatile stimulation determines timing and specificity of NF- $\kappa$ B-dependent transcription'. *Science* (2009) 324:242–6. doi: 10.1126/science.1164860

10. Tay S, Hughey JJ, Lee TK, Lipniacki T, Quake SR, Covert MW. 'Single-cell NF-kappaB dynamics reveal digital activation and analogue information processing'. *Nature* (2010) 466:267–71. doi: 10.1038/nature09145
11. Son M, Wang AG, Tu HL, Metzlg MO, Patel P, Husain K, et al. 'NF-kappaB responds to absolute differences in cytokine concentrations'. *Sci Signaling* (2021) 14(666):eaaz4382. doi: 10.1126/scisignal.aaz4382
12. Dorrington MG, Fraser IDC. 'NF-kB signaling in macrophages: Dynamics, crosstalk, and signal integration'. *Front Immunol* (2019) 10. doi: 10.3389/fimmu.2019.00705
13. Platanias LC. 'Mechanisms of type-I and type-II-interferon-mediated signalling'. *Nat Rev Immunol* (2005) 5:375–86. doi: 10.1038/nri1604
14. Ivashkiv LB. 'IFN-gamma: signalling, epigenetics and roles in immunity, metabolism, disease and cancer immunotherapy'. *Nat Rev Immunol* (2018) 18:545–58. doi: 10.1038/s41577-018-0029-z
15. Epelman S, Lavine KJ, Randolph GJ. 'Origin and functions of tissue macrophages'. *Immunity* (2014) 41:21–35. doi: 10.1016/j.immuni.2014.06.013
16. Villarino AV, Kanno Y, O'Shea JJ. 'Mechanisms and consequences of jak-STAT signaling in the immune system'. *Nat Immunol* (2017) 18:374–84. doi: 10.1038/ni.3691
17. Barrat FJ, Crow MK, Ivashkiv LB. 'Interferon target-gene expression and epigenomic signatures in health and disease'. *Nat Immunol* (2019) 20:1574–83. doi: 10.1038/s41590-019-0466-2
18. Van Eyndhoven LC, Singh A, Tel J. 'Decoding the dynamics of multilayered stochastic antiviral IFN-I responses'. *Trends Immunol* (2021) 42:824–39. doi: 10.1016/j.it.2021.07.004
19. Dalton DK, Pitts-Meek S, Keshav S, Figari IS, Bradley A, Stewart TA. 'Multiple defects of immune cell function in mice with disrupted interferon-gamma genes'. *Science* (1993) 259:1739–42. doi: 10.1126/science.8456300
20. Jouanguy E, Altare F, Lamhamedi-Cherradi S, Casanova JL. 'Infections in IFNGR-1-deficient children'. *J Interferon Cytokine Res* (1997) 17:583–7. doi: 10.1089/jir.1997.17.583
21. Payen D, Faivre V, Miatello J, Leentjens J, Brumpt C, Tissières P, et al. 'Multicentric experience with interferon gamma therapy in sepsis induced immunosuppression. a case series'. *BMC Infect Dis* (2019) 19:931. doi: 10.1186/s12879-019-4526-x
22. Blanco-Melo D, Nilsson-Payant BE, Liu WC, Uhl S, Hoagland D, Moller R, et al. 'Imbalanced host response to SARS-CoV-2 drives development of COVID-19'. *Cell* (2020) 181:1036–45.e9. doi: 10.1016/j.cell.2020.04.026
23. Lee JS, Shin EC. 'The type I interferon response in COVID-19: implications for treatment'. *Nat Rev Immunol* (2020) 20:585–86. doi: 10.1038/s41577-020-00429-3
24. Bach EA, Szabo SJ, Dighe AS, Ashkenazi A, Aguet M, Murphy KM, et al. 'Ligand-induced autoregulation of IFN-gamma receptor beta chain expression in T helper cell subsets'. *Science* (1995) 270:1215–8. doi: 10.1126/science.270.5239.1215
25. Kok F, Rosenblatt M, Teusel M, Nizharadze T, Goncalves Magalhaes V, Dachert C, et al. 'Disentangling molecular mechanisms regulating sensitization of interferon alpha signal transduction'. *Mol Syst Biol* (2020) 16:e8955. doi: 10.15252/msb.20198955
26. Mudra A, Jiang Y, Arimoto KI, Xu B, Rajesh A, Ryan AP, et al. 'Cell-cycle-gated feedback control mediates desensitization to interferon stimulation'. *Elife* (2020) 9:e58825. doi: 10.7554/eLife.58825
27. Yasukawa H, Sasaki A, Yoshimura A. 'Negative regulation of cytokine signaling pathways'. *Annu Rev Immunol* (2000) 18:143–64. doi: 10.1146/annurev.immunol.18.1.143
28. Liau NPD, Laktyushin A, Lucet IS, Murphy JM, Yao S, Whitlock E, et al. 'The molecular basis of JAK/STAT inhibition by SOCS1'. *Nat Commun* (2018) 9:1558. doi: 10.1038/s41467-018-04013-1
29. Smieja J, Jamaluddin M, Brasier AR, Kimmel M. 'Model-based analysis of interferon-β induced signaling pathway'. *Bioinformatics* (2008) 24:2363–69. doi: 10.1093/bioinformatics/btn400
30. Böhmer F-D, Karlheinz F. 'Protein tyrosine phosphatases as wardens of STAT signaling'. *JAK-STAT* (2014) 3:e28087–e87. doi: 10.4161/jkst.28087
31. Netea MG, Dominguez-Andres J, Barreiro LB, Chavakis T, Divangahi M, Fuchs E, et al. 'Defining trained immunity and its role in health and disease'. *Nat Rev Immunol* (2020) 20:375–88. doi: 10.1038/s41577-020-0285-6
32. Kamada R, Yang W, Zhang Y, Patel MC, Yang Y, Ouda R, et al. 'Interferon stimulation creates chromatin marks and establishes transcriptional memory'. *Proc Natl Acad Sci U.S.A.* (2018) 115:E9162–E71. doi: 10.1073/pnas.1720930115
33. Hu X, Herrero C, Li WP, Antoniv TT, Falck-Pedersen E, Koch AE, et al. 'Sensitization of IFN-gamma jak-STAT signaling during macrophage activation'. *Nat Immunol* (2002) 3:859–66. doi: 10.1038/ni828
34. Morris MC, Gilliam EA, Li L. 'Innate immune programming by endotoxin and its pathological consequences'. *Front Immunol* (2014) 5:680. doi: 10.3389/fimmu.2014.00680.
35. Buckley JM, Wang JH, Redmond HP. 'Cellular reprogramming by gram-positive bacterial components: a review'. *J Leukoc Biol* (2006) 80:731–41. doi: 10.1189/jlb.0506312
36. Sakamoto S, Qin J, Navarro A, Gamero A, Potla R, Yi T, et al. 'Cells previously desensitized to type 1 interferons display different mechanisms of activation of stat-dependent gene expression from naive cells'. *J Biol Chem* (2004) 279:3245–53. doi: 10.1074/jbc.M309631200
37. Hornung V, Bauernfeind F, Halle A, Samstad EO, Kono H, Rock KL, et al. 'Silica crystals and aluminum salts activate the NALP3 inflammasome through phagosomal destabilization'. *Nat Immunol* (2008) 9:847–56. doi: 10.1038/ni.1631
38. Bagnall J, Boddington C, Boyd J, Brignall R, Rowe W, Jones NA, et al. 'Quantitative dynamic imaging of immune cell signalling using lentiviral gene transfer'. *Integr Biol* (2015) 7:713–25. doi: 10.1039/c5ib00067j
39. Brignall R, Cauchy P, Bevington SL, Gorman B, Pisco AO, Bagnall J, et al. 'Integration of kinase and calcium signaling at the level of chromatin underlies inducible gene activation in T cells'. *J Immunol* (2017) 199(8):2652–67. doi: 10.4049/jimmunol.1602033
40. Satoh J, Tabunoki H. 'A comprehensive profile of ChIP-Seq-Based STAT1 target genes suggests the complexity of STAT1-mediated gene regulatory mechanisms'. *Gene Regul Syst Bio* (2013) 7:41–56. doi: 10.4137/GRSB.S11433
41. Orjalo AV Jr., Johansson HE. 'Stellaris(R) RNA fluorescence *In situ* hybridization for the simultaneous detection of immature and mature long noncoding RNAs in adherent cells'. *Methods Mol Biol* (2016) 1402:119–34. doi: 10.1007/978-1-4939-3378-5\_10
42. Tzanov N, Samacoits A, Chouaib R, Traboulsi AM, Gostan T, Weber C, et al. 'smiFISH and FISH-quant - a flexible single RNA detection approach with super-resolution capability'. *Nucleic Acids Res* (2016) 44:e165. doi: 10.1093/nar/gkw784
43. Livak KJ, Schmittgen TD. 'Analysis of relative gene expression data using real-time quantitative PCR and the 2<sup>-ΔΔC<sub>T</sub></sup> method'. *Methods* (2001) 25:402–8. doi: 10.1006/meth.2001.1262
44. Nelson DE, Ihekwaba AEC, Elliott M, Johnson JR, Gibney CA, Foreman BE, et al. 'Oscillations in NF-kappa b signaling control the dynamics of gene expression'. *Science* (2004) 306:704–08. doi: 10.1126/science.1099962
45. Hoffmann A, Levchenko A, Scott ML, Baltimore D. 'The IkappaB-NF-kappaB signaling module: temporal control and selective gene activation'. *Science* (2002) 298:1241–5. doi: 10.1126/science.1071914
46. Lee RE, Walker SR, Savery K, Frank DA, Gaudet S. 'Fold change of nuclear NF-kappaB determines TNF-induced transcription in single cells'. *Mol Cell* (2014) 53:867–79. doi: 10.1016/j.molcel.2014.01.026
47. Kardynska M, Paszek A, Smieja J, Spiller D, Widlak W, White MRH, et al. 'Quantitative analysis reveals crosstalk mechanisms of heat shock-induced attenuation of NF-kappa b signaling at the single cell level'. *PLoS Comput Biol* (2018) 14(4):e1006130. doi: 10.1371/journal.pcbi.1006130
48. Patel P, Drayman N, Liu P, Bilgic M, Tay Savaş. 'Computer vision reveals hidden variables underlying NF-kB activation in single cells'. *Sci Adv* (2021) 7:eabg4135. doi: 10.1126/sciadv.abg4135
49. Topolewski P, Zakrzewska KE, Walczak Jaroslaw, Nienaltowski K, Müller-Newen G, Singh A, et al. 'Phenotypic variability, not noise, accounts for most of the cell-to-cell heterogeneity in IFN-γ and oncostatin m signaling responses'. *Sci Signaling* (2022) 15:eabd9303. doi: 10.1126/scisignal.abd9303
50. Lamaze C, Blouin Cédric. Interferon gamma receptor: The beginning of the journey. *Front Immunol* (2013) 4. doi: 10.3389/fimmu.2013.00267
51. Krause CD, He W, Kotenko S, Pestka S. 'Modulation of the activation of Stat1 by the interferon-gamma receptor complex'. *Cell Res* (2006) 16:113–23. doi: 10.1038/sj.cr.7310015
52. Bensaude O. 'Inhibiting eukaryotic transcription: Which compound to choose? how to evaluate its activity?'. *Transcription* (2011) 2:103–08. doi: 10.4161/trns.2.3.16172
53. Mowen K, David M. 'Regulation of STAT1 nuclear export by Jak1'. *Mol Cell Biol* (2000) 20:7273–81. doi: 10.1128/MCB.20.19.7273-7281.2000
54. Begitt A, Meyer T, Rossum Mv, Vinkemeier U. 'Nucleocytoplasmic translocation of Stat1 is regulated by a leucine-rich export signal in the coiled-coil domain'. *Proc Natl Acad Sci* (2000) 97:10418–23. doi: 10.1073/pnas.190318397
55. van der Watt PJ, Leaner VD. 'The nuclear exporter, Crm1, is regulated by NFY and Sp1 in cancer cells and repressed by p53 in response to DNA damage'. *Biochim Biophys Acta* (2011) 1809:316–26. doi: 10.1016/j.bbagr.2011.05.017
56. Heinson KM, Bourdeau A, Doody KM, Tremblay ML. 'Protein tyrosine phosphatases PTP-1B and TC-PTP play nonredundant roles in macrophage

development and IFN-gamma signaling'. *Proc Natl Acad Sci U.S.A.* (2009) 106:9368–72. doi: 10.1073/pnas.0812109106

57. Pertsovskaya I, Abad E, Domedel-Puig N, Garcia-Ojalvo J, Villoslada P. 'Transient oscillatory dynamics of interferon beta signaling in macrophages'. *BMC Syst Biol* (2013) 7:59. doi: 10.1186/1752-0509-7-59
58. Prakash SJ, Li Y, Chen Y-Y, Hsu S-TD, Page R, Peti W, et al. 'The catalytic activity of TCPTP is auto-regulated by its intrinsically disordered tail and activated by integrin alpha-1'. *Nat Commun* (2022) 13:94. doi: 10.1038/s41467-021-27633-6
59. Simoncic PD, Lee-Loy A, Barber DL, Tremblay ML, McGlade CJ. 'The T cell protein tyrosine phosphatase is a negative regulator of janus family kinases 1 and 3'. *Curr Biol* (2002) 12:446–53. doi: 10.1016/S0960-9822(02)00697-8
60. ten Hoeve J, de Jesus Ibarra-Sanchez M, Fu Y, Zhu W, Tremblay M, David M, et al. 'Identification of a nuclear Stat1 protein tyrosine phosphatase'. *Mol Cell Biol* (2002) 22:5662–8. doi: 10.1128/MCB.22.16.5662-5668.2002
61. Londino JD, Gulick DL, Lear TB, Suber TL, Weathington NM, Masa LS, et al. 'Post-translational modification of the interferon-gamma receptor alters its stability and signaling'. *Biochem J* (2017) 474:3543–57. doi: 10.1042/BCJ20170548
62. Marijanovic Z, Ragimbeau J, Kumar KGS, Fuchs SY, Pellegrini S. 'TYK2 activity promotes ligand-induced IFNAR1 proteolysis'. *Biochem J* (2006) 397:31–8. doi: 10.1042/BJ20060272
63. Kumar KGS, Tang W, Ravindranath AK, Clark WA, Croze Ed, Fuchs SY. 'SCFHOS ubiquitin ligase mediates the ligand-induced down-regulation of the interferon- $\alpha$  receptor'. *EMBO J* (2003) 22:5480–90. doi: 10.1093/emboj/cdg524
64. Zanin N, de Lesegno CV, Lamaze C, Blouin CM. 'Interferon receptor trafficking and signaling: Journey to the cross roads'. *Front Immunol* (2021) 11:615603–03. doi: 10.3389/fimmu.2020.615603
65. Pike KA, Tremblay ML. 'TC-PTP and PTP1B: Regulating JAK-STAT signaling, controlling lymphoid malignancies'. *Cytokine* (2016) 82:52–7. doi: 10.1016/j.cyto.2015.12.025
66. Lyashenko E, Niepel M, Dixit PD, Lim SK, Sorger PK, Vitkup D. 'Receptor-based mechanism of relative sensing and cell memory in mammalian signaling networks'. *Elife* (2020) 9:e50342. doi: 10.7554/eLife.50342
67. Takaoka A, Mitani Y, Suemori H, Sato M, Yokochi T, Noguchi S, et al. 'Cross talk between interferon-gamma and -alpha/beta signaling components in caveolar membrane domains'. *Science* (2000) 288:2357–60. doi: 10.1126/science.288.5475.2357
68. Rayamajhi M, Humann J, Penheiter K, Andreasen K, Lenz LL. 'Induction of IFN- $\alpha$  enables listeria monocytogenes to suppress macrophage activation by IFN- $\gamma$ '. *J Exp Med* (2010) 207:327–37. doi: 10.1084/jem.20091746
69. Lehtonen A, Matikainen S, Julkunen I. 'Interferons up-regulate STAT1, STAT2, and IRF family transcription factor gene expression in human peripheral blood mononuclear cells and macrophages'. *J Immunol* (1997) 159:794–803.
70. Sung M-H, Li N, Lao Q, Gottschalk RA, Hager GL, Fraser IDC. 'Switching of the relative dominance between feedback mechanisms in lipopolysaccharide-induced NF- $\kappa$ B signaling'. (2014) 7(308):ra6–6. doi: 10.1126/scisignal.2004764
71. Bagnall J, Boddington C, England H, Brignall R, Downton P, Alsoufi Z, et al. 'Quantitative analysis of competitive cytokine signaling predicts tissue thresholds for the propagation of macrophage activation'. *Sci Signaling* (2018) 11(540):eaaf3998. doi: 10.1126/scisignal.aaf3998
72. Bagnall J, Rowe W, Alachkar N, Roberts J, England H, Clark C, et al. 'Gene-specific linear trends constrain transcriptional variability of the toll-like receptor signaling'. *Cell Syst* (2020) 11:300–14.e8. doi: 10.1016/j.cels.2020.08.007